Supporting Information

Tuning Rashba Spin-Orbit Coupling in Gated Multi-layer InSe

Kasun Premasiri, [†] *Santosh Kumar Radha,* [†] *Sukrit Sucharitakul,* [†] *U. Rajesh Kumar,* [‡] *Raman Sankar,* [‡,§] *Fang-Cheng Chou,* [‡] *Yit-Tsong Chen,* [#,¶] *and Xuan P. A. Gao** [†]

[†]Department of Physics, Case Western Reserve University, 2076 Adelbert Road, Cleveland, OH 44106, USA.

[‡]Center for Condensed Matter Sciences, National Taiwan University, Taipei 10617, Taiwan.

[§]Institute of Physics, Academia Sinica, Taipei 11529, Taiwan.

[#]Department of Chemistry, National Taiwan University, Taipei 10617, Taiwan.

[¶]Institute of Atomic and Molecular Sciences, Academia Sinica, Taipei 10617, Taiwan.

*Corresponding author: xuan.gao@case.edu

1. Materials and Methods

InSe Crystal Growth:

Bridgman method was used to grow bulk InSe crystals.[1] Purity of the In and Se sources (Sigma-Aldrich®) used was 99.999%, leading to single-crystalline and pristine InSe. A quartz ampule was utilized for the synthesis of crystals. An admixture of In and Se compounds was placed at one end of the ampule, and then the ampule was evacuated to about 10^{-4} Pa, after sealing the other end of the ampule. Homogenization of the mixture was conducted in a horizontal furnace at 600 °C for 48 hours. The as-grown crystals were easily-exfoliable, and showed good crystal quality.

SEM (Figure 1c):

A TESCAN VEGA3® scanning electron microscope (SEM) was used to obtain the micrograph of the sample as shown in Fig. 1c.

AFM (Figure 1d):

An Agilent 5500® atomic force microscope (AFM) was used to obtain the thickness profile of the sample as shown in Fig. 1d.

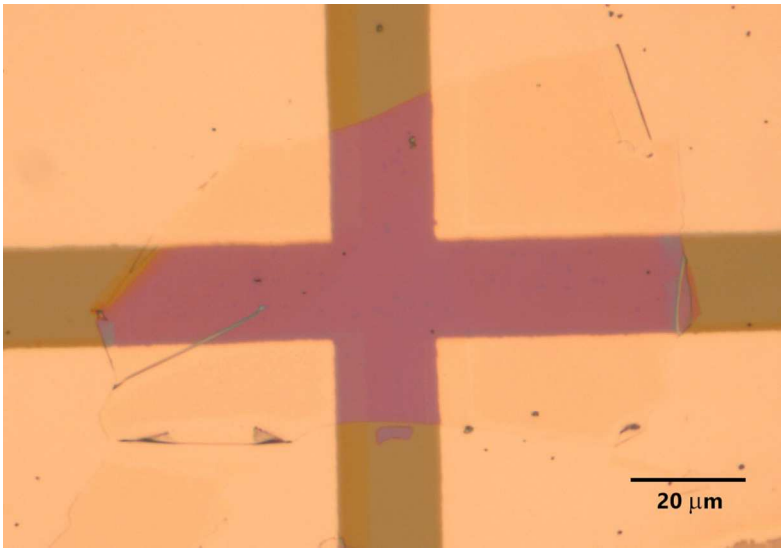

Figure S1: An optical micrograph of the sample used for the magnetoconductance study.

2. Device Geometry and Hall Measurement

van der Pauw geometry was utilized in fabricating InSe devices for this study.[2] Figure S2 illustrates how the longitudinal and transverse magneto-resistances R_{xx} and R_{xy} were extracted. Since it is possible to have some mixing between R_{xx} and R_{xy}, especially with the van der Pauw geometry, all the magneto-transport measurements were symmetrized for R_{xx} and anti-symmetrized for R_{xy}. To remove the mixing of antisymmetric R_{xy} in the measured R_{xx}, R_{xx} was symmetrized using:

$$R_{xx} = \frac{R_{xx}(B) + R_{xx}(-B)}{2}$$

and similarly, R_{xy} was anti-symmetrized using:

$$R_{xy} = \frac{R_{xy}(B) - R_{xy}(-B)}{2}.$$

Figure S3 depicts the effect of symmetrization on magneto-resistance results. As shown in Fig.S3, the raw $R_{xx}(B)$ data (red line) contained some anti-symmetric component due to the mixing of R_{xy} signal. After the symmetrization, $R_{xx}(B)$ becomes symmetric (green line). The low magnetic field $R_{xx}(B)$ is due to the weak antilocalization effect as discussed in the main manuscript while the behavior of $R_{xx}(B)$ at high fields (B > ~1T) appears to be similar to the negative parabolic magneto-resistance caused by electron-electron interaction effect in 2D systems[3]. R_{xx} and R_{xy} values were converted to corresponding resistivity values for a two-dimensional flake measured in the van der Pauw geometry: $\rho_{xx} = R_{xx}\ \pi/\ln(2)$ and $\rho_{xy} = R_{xy}$. Then these ρ_{xx} and ρ_{xy} values

were used to extract the corresponding conductivity values by inverting the magneto-resistivity tensor using the following equations.

$$\sigma_{xx} = \frac{\rho_{xx}}{\rho_{xx}^2 + \rho_{xy}^2}$$

$$\sigma_{xy} = \frac{\rho_{xy}}{\rho_{xx}^2 + \rho_{xy}^2}$$

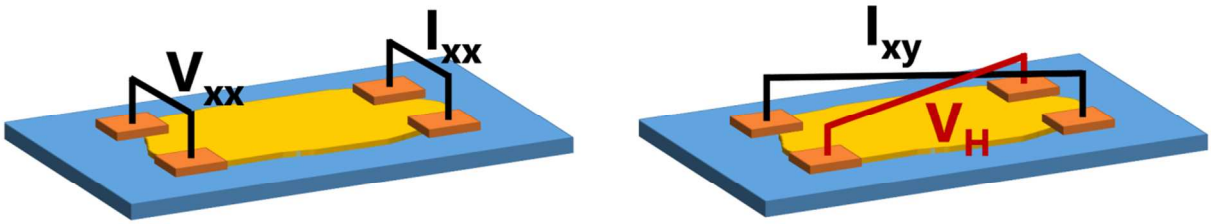

Figure S2: Schematic of the longitudinal and transverse (Hall) magnetoresistance measurements.

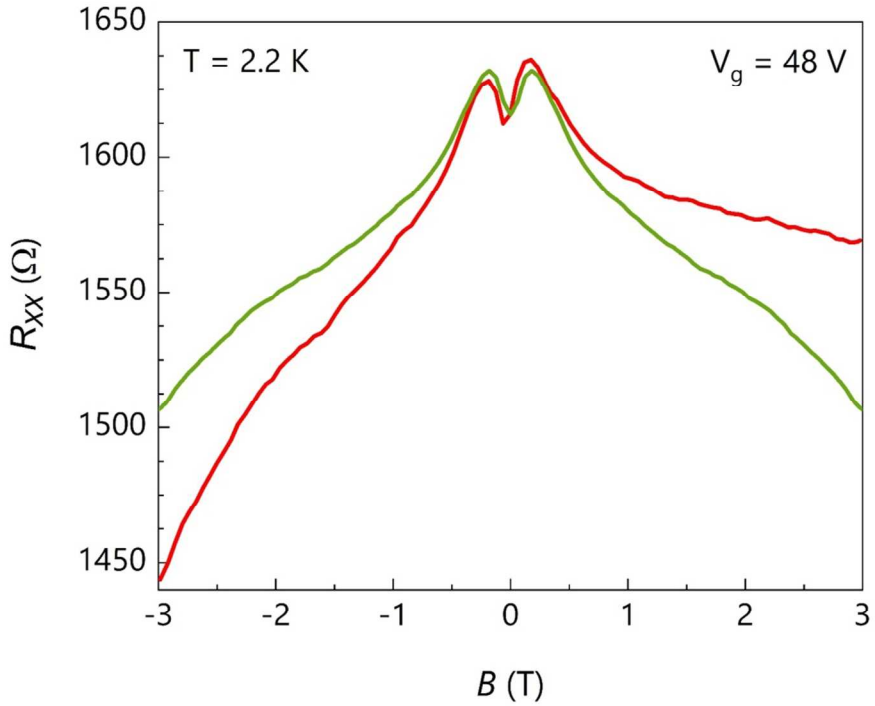

Figure S3: R_{xx} vs. B at 2.2 K (when V_g = 48 V) before (red line) and after (green line) symmetrization to remove the mixing of anti-symmetric R_{xy}.

Once the possibility of mixing is accounted for using symmetrization and anti-symmetrization, this geometry can be adequately used to perform a more accurate Hall measurement.

The Hall voltage (V_H) was calculated using:

$$V_H = \frac{R_H I B}{t}$$

where R_H is the Hall coefficient, I is the corresponding current, B is the magnetic field and t is the thickness of the sample. Then the corresponding mobility (μ) and carrier density (n) values were extracted using the following two equations.

$$n = \frac{1}{R_H e}$$

$$\mu = \frac{R_H}{\rho}$$

where ρ is the resistivity.

Reliability of the Hall measurement from this approach can be tested by calculating the carrier density using the gate capacitance, and then comparing that with the carrier density extracted from the Hall measurement. The gate capacitance generated by the Si_3N_4 layer is,

$$C_{Si_3N_4} = \frac{\varepsilon_{Si_3N_4}\varepsilon_0 A}{d}$$

where, $\varepsilon_{Si_3N_4}$ is the dielectric constant of Si_3N_4 (= 7.5), A is the cross-sectional area of the sample, and d is the thickness of the Si_3N_4 layer. This leads to $C_{Si_3N_4} = 44.25$ nF cm^{-2}. Then the carrier density corresponding to this gate capacitance at different gate voltages can be calculated using,

$$n = C_{Si_3N_4} V_g$$

This is assuming the quantum capacitance is much smaller than $C_{Si_3N_4}$. The carrier density values extracted this way are plotted with the corresponding carrier density values from the Hall measurement in Figure S4. It can be seen that there is a good consistency between the Hall density and the estimated carrier density using gate capacitance.

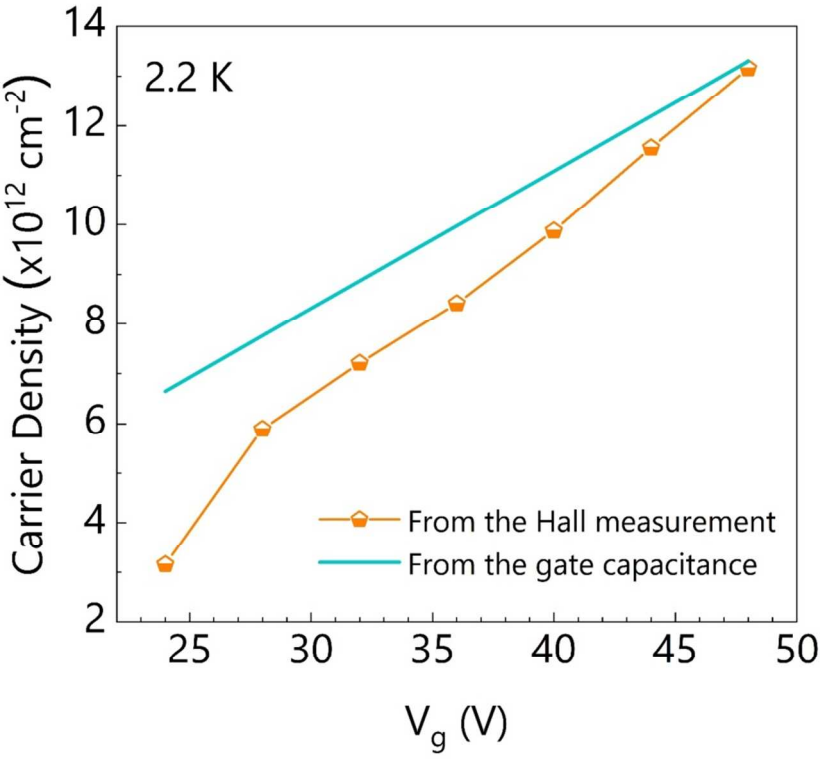

Figure S4: The measured carrier density extracted from the Hall effect and the calculated carrier density using the geometrical gate capacitance at various gate voltages at 2.2 K.

3. Energy Band Diagram Calculations

To get the energy band diagrams, Schrödinger and Poisson's equations were solved self-consistently. Poisson's equation was solved using an equation solver [4] (which is freely available) in compliance with the boundary conditions of the system. Schrödinger equation was solved using a python code written by us. To maintain the self-consistency, those two resources were used in tandem for the calculation. Material properties of InSe, Si_3N_4 and Si utilized in the energy band diagram calculations are given in the Supplementary Table S1. As for the anisotropic properties, they were included after the requisite averaging.

Poisson's equation can be used to describe the electrostatics of the FET structure:

$$\varepsilon \nabla_x^2 \varphi(x) = -\rho(x)$$

where, $\varphi(x)$ is the electrostatic potential, and ε is the dielectric constant of the material. Then the charge density ($\rho(x)$) of the structure can be decomposed into:

$$\rho(x) = q_0[p(x) - n(x) - N_a(x) + N_d(x)]$$

where, $p(x)$ and $n(x)$ are the hole and electron densities, respectively. $N_a(x)$ and $N_d(x)$ are ionized acceptor and donor concentrations, respectively.

Material	Bandgap (eV)	Dielectric Constant	Electron Effective Mass (m_e)	Electron Affinity (eV)
InSe	1.28	10.9	0.14	4.55
Si_3N_4	5.0	7.5	0.45	1.8
Si	1.12	11.9	1.1	4.05

Supplementary Table S1: Material properties of InSe, Si_3N_4 and Si utilized in the energy band diagram calculations.

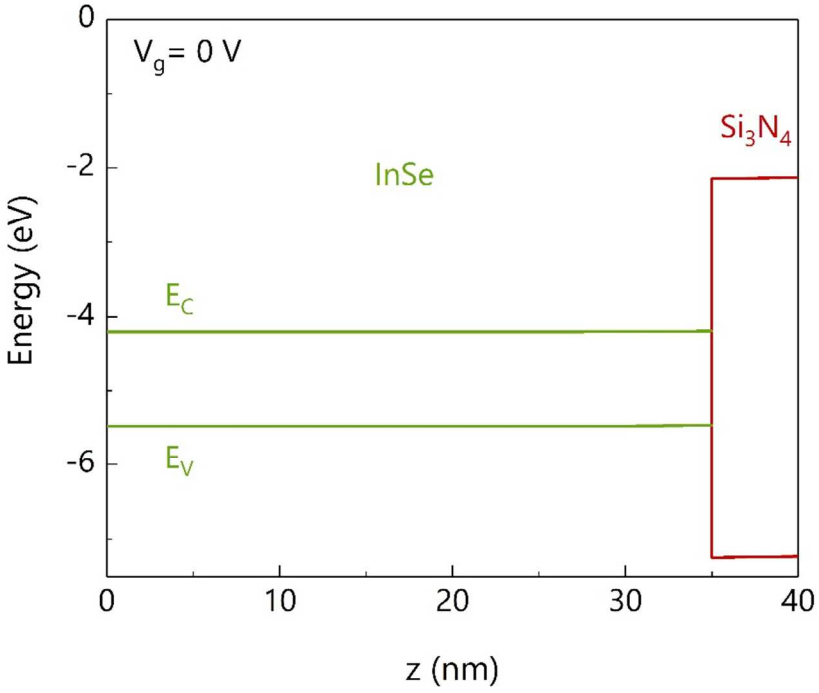

Figure S5: The energy band diagram of InSe at V_g=0 V.

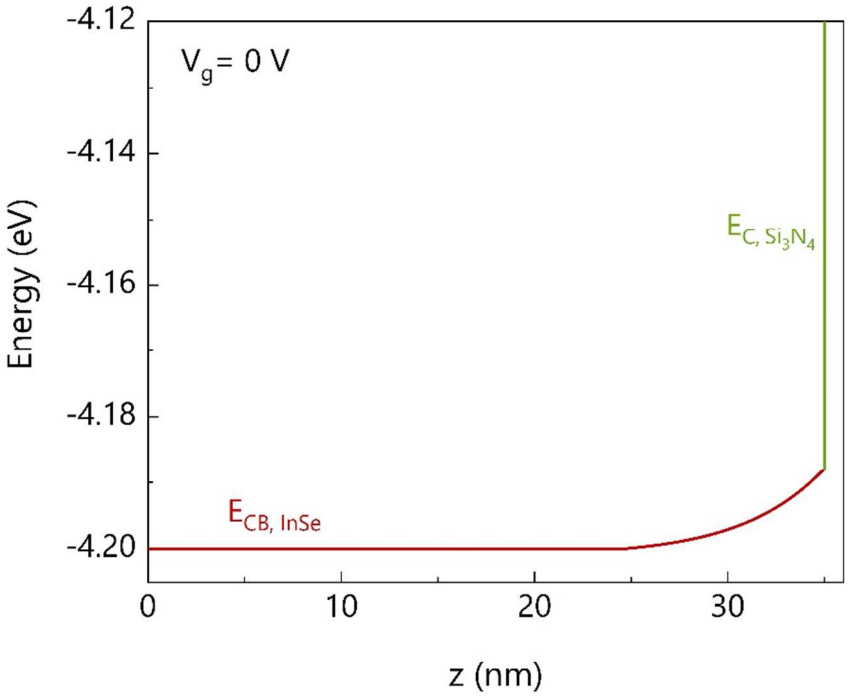

Figure S6: The conduction band edge variation in Figure S5 plotted in an expanded scale.

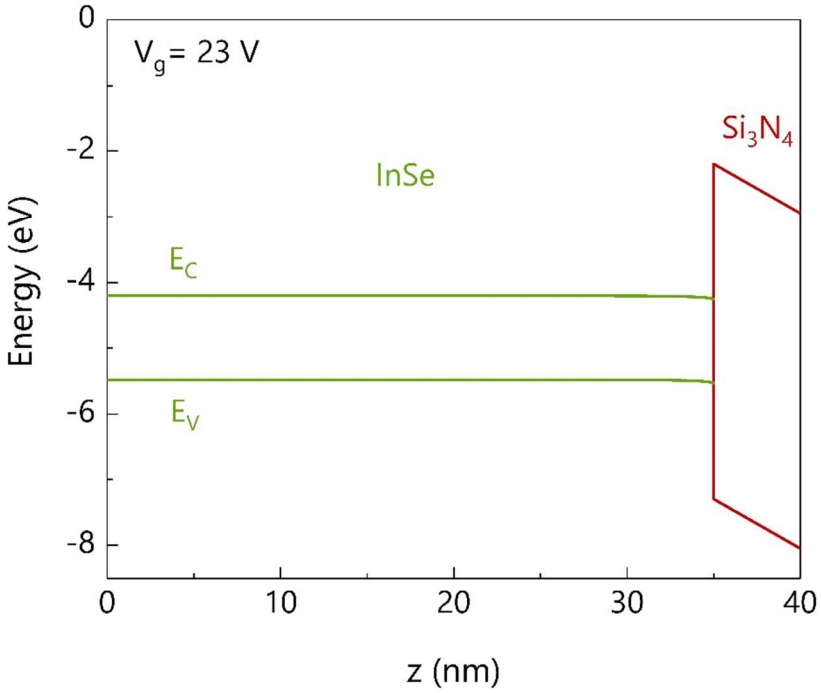

Figure S7: The energy band diagram of InSe at V_g = 23 V.

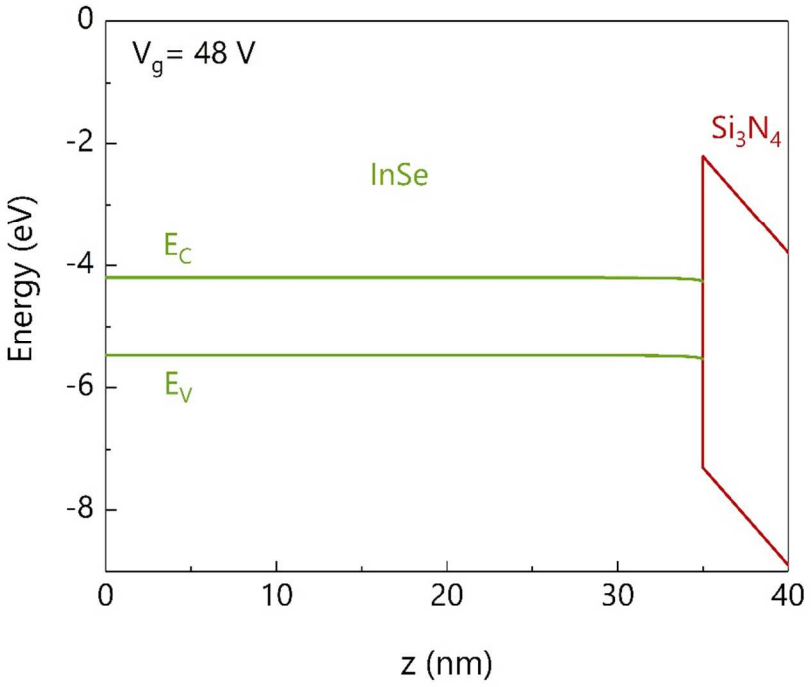

Figure S8: The energy band diagram of InSe at V_g = 48 V.

REFERENCES

1 Tamalampudi, S. R.; Lu, Y.-Y.; U., R. K.; Sankar, R.; Liao, C.-D.; B., K. M.; Cheng, C.-H.; Chou, F. C.; Chen, Y.-T. *Nano Letters* **2014**, *14*(5), 2800–2806.

2 van der Pauw, L.J. *Philips Research Reports* **1958**, 13, 1–9.

3 Paalanen, M. A., Tsui, D. C. and Hwang, J. C. M. *Phys. Rev. Lett.* **1983,** *51*, 2226.

4 1D Poisson: https://www3.nd.edu/~gsnider/